Arabian Journal of Chemistry (2023) **16**, 105194

King Saud University

Arabian Journal of Chemistry

www.ksu.edu.sa
www.sciencedirect.com

ORIGINAL ARTICLE

Enhanced *in vivo* wound healing efficacy and excellent antibacterial, antifungal, antioxidant and anticancer activities via AgNPs@*PCS*

Majid Zare-Bidaki [a,1], Alireza Ghasempour [b,1], Pouria Mohammadparast-Tabas [b,1], Seyedeh Masoumeh Ghoreishi [c], Esmat Alamzadeh [a], Reyhane Javanshir [b], Binh Nguyen Le [d,e], Mahsa Barakchi [b], Mehdi Fattahi [d,e,*], Sobhan Mortazavi-Derazkola [f,*]

[a] *Infectious Diseases Research Center, Birjand University of Medical Sciences, Birjand, Iran*
[b] *Student Research Committee, Birjand University of Medical Sciences, Birjand, Iran*
[c] *Cellular and Molecular Biology Research Center, Health Research Institute, Babol University of Medical Sciences, Babol, Iran*
[d] *Institute of Research and Development, Duy Tan University, Da Nang, Vietnam*
[e] *School of Engineering & Technology, Duy Tan University, Da Nang, Vietnam*
[f] *Medical Toxicology and Drug Abuse Research Center (MTDRC), Birjand University of Medical Sciences, Birjand, Iran*

Received 14 March 2023; accepted 22 July 2023
Available online 28 July 2023

KEYWORDS

Silver nanoparticle;
Antioxidant;
Antibacterial;
Anticancer;
Petroselinum crispum;
Wound healing

Abstract Today, wound healing is an important clinical problem that is often affected by microbial infection and not paying attention to this problem can cause irreparable damage to people. Biosynthesis of metal nanoparticles (NPs) has created a huge revolution in the field of nanomedicine due to their non-toxic, biocompatible, and stable characteristics. For this purpose, in this study, *Petroselinum crispum* seed extract (PCS) was applied to preparation of silver nanoparticles (AgNPs@*PCS*). The optimization of the silver nanoparticle synthesis involved adjusting the concentration of the silver salt, as well as the time and temperature parameters. After identifying the fabricated nanoparticles by FESEM, XRD, FT-IR, UV–Vis, TEM and EDS, their biological activity (like antibacterial, antifungal, antioxidant, anticancer, and wound treatment) was determined. The green synthesis of AgNPs was confirmed by several characteristics, including the surface plasmon response with a peak around 420 nm, the presence of both regular and heterogeneous sizes in the sample, and the observed color change from a clear solution to a brown color. The

* Corresponding authors.
E-mail addresses: Mehdifattahi@duytan.edu.vn (M. Fattahi), S.mortazavi23@yahoo.com (S. Mortazavi-Derazkola).
[1] These authors contributed equally to this work.

Peer review under responsibility of King Saud University.

Production and hosting by Elsevier

https://doi.org/10.1016/j.arabjc.2023.105194

antimicrobial properties of the biofabricated AgNPs were investigated against fungal and various bacteria. The anticancer property of AgNPs@*PCS* was demonstrated by an IC50 value of 200 µg/ml after a 24-hour exposure on the MCF-7 cell line. Also, a dose-dependent antioxidant performance of AgNPs was found against the DPPH free radical. Histopathological evaluations of AgNPs@*PCS* ointment illustrated significant decrease in inflammatory cells. The results showed that vaseline ointment containing AgNPs@*PCS* prevented inflammation in the wound area and increased the number of fibroblast cells, which led to accelerated wound healing. Furthermore, in-vivo investigation showed the higher percentage of wound closure on days 7 and 14 was than the control group (Vaseline). Interestingly, the wound was completely closed after 21 days. Thus, we concluded that *Petroselinum crispum*-mediated silver nanoparticles show potential biological activity which can be used as nano-drug in clinical treatment.

1. Introduction

Since burn is the most widespread type of soft tissue injury that can put patient's life in danger if left untreated, burn treatment has attracted a lot of attention in the field of medicine. Due to this, the achieving of effective and powerful pharmaceuticals in the treatment of burn wounds has been considered (Oryan et al., 2017; Wang et al., 2018). In the study of Richard & co-workers, nano-fiber threads were fabricated with curcumin and it was observed that the use of these fabricated nano-fiber threads in suturing the wounds of rats leads to faster healing of the wounds (Richard and Verma, 2021). Also, Qianqian *et al*. studied hydrogel synthesis with the help of Tilapia peptides and hydroxyapatite and chitosan system and investigated its effects in burn wound healing. They observed that the fabricated hydrogel, in addition to being compatible with endothelial cells, by reducing the expression of TNF-α and IL-6 and increasing the expression of collagen, STAT 3 and VEGF, strengthens skin epithelial tissue regeneration (Qianqian et al., 2021). Over the recent years, nanotechnology has significantly influenced diverse fields, including pharmaceuticals (Mortazavi-Derazkola et al., 2016), environment (Shirzadi-Ahodashti et al., 2021), medicine (Mohammadzadeh et al., 2019), and etc. Nanoparticles (NP) are a substance that has a dimension between 1 and 100 nm in size (Ebrahimzadeh et al., 2020). Applications of nanomaterials include their use in pharmaceuticals and drug delivery, environmental health and medicine (Rafique et al., 2017; Naghdipari et al., 2019). Zheng & co-workers fabricated solid lipid nnaoparticles as a delivery carrier for doxorubicin that was sensitive to pH. In-vitro and in-vivo investigation, revealed that the reported nano-system can lead to improved cancer treatment (Zheng et al., 2019). Hasan and colleagues conducted a study where they fabricated zinc oxide nanoparticles utilizing Withania coagulans extract. The research aimed to evaluate the antibacterial effects of the fabricated nanoparticles against *Staphylococcus aureus* and *Pseudomonas aeruginosa* bacteria. The results demonstrated high antibacterial properties of the ZnO NPs against the selected bacteria, indicating their effectiveness in inhibiting the growth of these bacterial strains (Hasan et al., 2021).

Silver nanoparticles (AgNPs) possess various physical and chemical properties, as well as desirable electrical and thermal conductivity. In comparison to other nanoparticles like gold (Au) (Suchomel et al., 2018), copper (Cu) (Jayarambabu et al., 2020), iron (Fe) (Perveen et al., 2022), palladium (Pd) (Veisi et al., 2019), copper oxide (CuO) (Waris et al., 2021), zinc oxide (ZnO) (Doan Thi et al., 2020), and nickel oxide (NiO) (Sabouri et al., 2021), AgNPs exhibit distinct advantages and hold a more significant position. These advantages are attributed to their unique size, which confers special properties that make them stand out among other metals and semiconductor materials (Zhang et al., 2016; Hussain et al., 2016). The AgNPs have a wide range of applications, including catalytic activity, energy production, antibacterial, antifungal, and anti-inflammatory activity (Burduşel et al., 2018; Yaqoob et al., 2020; Ahmad et al., 2019). Several studies have highlighted the significant role of silver nanoparticles (AgNPs) in the field of medicine, particularly in wound healing and burn injuries (Ramadhan et al., 2021; Abbasi et al., 2021). Tyavambiza and colleagues conducted a study where they fabricated silver nanoparticles (AgNPs) utilizing *Cotyledon orbiculata* plant extract. The research aimed to investigate the potential antibacterial, antifungal, and anti-inflammatory effects of the fabricated nanoparticles. Their findings revealed that the AgNPs exhibited significant antibacterial and antifungal properties, effectively combating strains of *Staphylococcus aureus*, *Staphylococcus epidermidis*, *Pseudomonas aeruginosa*, and *Candida albicans*. Additionally, the fabricated AgNPs demonstrated anti-inflammatory capabilities by inhibiting the pro-inflammatory cytokine pathway (Tyavambiza et al., 2021). In the study conducted by Sood et al. (Sood and Chopra, 2018), silver nanoparticles were fabricated using *Ocimum sanctum* extract, and their effects on burn wounds were examined. The findings of the study revealed that the fabricated AgNPs significantly enhanced the process of wound healing, resulting in a 96% improvement compared to the control group. This suggests that the application of AgNPs derived from *Ocimum sanctum* extract holds great potential for improving the healing of burn wounds.

Nanoparticles are commonly fabricated by different methods, including evaporation–condensation (Zare-Bidaki et al., 2022), hydrothermal (Zhang et al., 2019), photochemical (Lin and Cheng, 2020), microwave process (Lalegani et al., 2020), biosynthesis (Ahmad et al., 2019), etc. The use of certain chemical and physical methods in various processes is known to incur high costs, consume significant amounts of energy, and potentially cause harm to the environment (Salem and Fouda, 2021). These methods often involve complex and resource-intensive procedures, as well as the use of chemicals or equipment that can contribute to environmental pollution and degradation. Currently, there is a growing emphasis on adopting a biocompatible approach that avoids any harmful effects. This has led to a notable focus on the green synthesis method, which has gained considerable attention for its potential to minimize the toxicity associated with nanoparticles. The most important reasons for increasing the tendency to green synthesis instead of using physical and chemical methods include environmental friendliness, cost-effectiveness, facile and fast, and its potential to reduce the toxicity of nanoparticles (Ebrahimzadeh et al., 2020; Salem and Fouda, 2021). Various studies have documented the synthesis of nanoparticles using a diverse range of organisms, including fungi, algae, bacteria, and plants. This preference is due to the presence of phytochemical compounds within these plant parts, which serve as stabilization, reduction, and capping agents during the synthesis process (Jadoun et al., 2021). Sharma *et al*. fabricated AgNPs using *Allium cepa* plant extract. The fabricated nanoparticles showed size range 36–98 nm in a spherical morphology with the zeta potential in the range of −12 to −26 mV (Sharma et al., 2018). In the study of Arassu *et al*.; AgNPs were fabricated by the green method

using *Pelargonium graveolens* plant extract. The fabricated nanoparticles had a spherical form and a size of about 164 nm. Data showed the antifungal effects of the biofabricated nanoparticles (Arassu et al., 2018).

In this study, parsley seeds were applied as a reducing agent. Parsley with the scientific name of *Petroselinum crispum* belongs to the Apiaceae family, in which different parts, including leaves, roots and seeds, are used in various industries (N. Mara de Menezes Epifanio, L. Rykiel Iglesias Cavalcanti, K. Falcão Dos Santos, P. Soares Coutinho Duarte, P. Kachlicki, M. Ożarowski, C. Jorge Riger, D. Siqueira de Almeida Chaves, 2020). Reducing and stabilizing effects of Parsley extract may contribute to these several bioactive substances (El-Borady et al., 2020). The medical and pharmaceutical applications and properties of parsley include use in gastrointestinal disorders, breast cancer, dermatitis, exanthema, kidney stone, diuretic, anti-inflammatory, and antioxidants (N. Mara de Menezes Epifanio, L. Rykiel Iglesias Cavalcanti, K. Falcão Dos Santos, P. Soares Coutinho Duarte, P. Kachlicki, M. Ożarowski, C. Jorge Riger, D. Siqueira de Almeida Chaves, 2020; El-Borady et al., 2020; Tang et al., 2015). In this research, a green synthesis approach was employed to synthesize AgNPs using the alcoholic extract of parsley seeds. Subsequently, the AgNPs that were prepared using this environmentally friendly method were evaluated for their potential in healing full-thickness burn wounds, as well as their antibacterial, antifungal, and antioxidant activities. This research introduces several distinct contributions in comparison to other studies, which can be summarized as follows: (i) The synthesis of noble metal nanoparticles in an environmentally friendly and straightforward manner. (ii) *Petroselinum crispum*-mediated AgNPs demonstrated remarkable effectiveness against bacteria, antioxidants, and fungi. (iii) AgNPs@*PCS* NPs exhibited significant anticancer properties specifically on the MCF-7 cell line. (iv) AgNPs@*PCS* NPs accelerated the process of wound healing. (v) In mice, AgNPs@*PCS* NPs enhanced the rate at which epidermal tissue formed.

2. Experimental

2.1. Materials

Silver nitrate ($AgNO_3$, 99.99%) was obtained from Merck, while methanol and DMSO were purchased from Sigma-Aldrich (St Louis, MO, USA). Gram-negative and gram-positive microorganisms were obtained from the Pasteur Institute of Iran. The Zantox kit, used to evaluate antioxidant capacity, was purchased from Kavosh Arian Azma Company. Ketamine (10%) and xylazine (2%) were obtained from Alfasan Company. Dulbecco's modified Eagle's medium (DMEM), trypsin-EDTA solution, 1% antibiotic–antimycotic solution, penicillin–streptomycin solution, and fetal bovine serum (FBS) were prepared by BIO IDEA in Iran. All experiments were conducted in triplicate, and deionized water was used as the solution in all processes.

2.2. Preparation of Petroselinum crispum seeds extracts

The extraction process was conducted according to the following procedure. Initially, *Petroselinum crispum* seeds were collected from Bagheran Mountains in the South Khorasan province of Iran. The collected seeds were then washed with sterile deionized water and dried. Subsequently, the prepared seeds were ground into a powder form. A quantity of 100 g of *Petroselinum crispum* was macerated in 1000 ml of methanol, serving as the solvent. The mixture was agitated at 150 rpm for duration of 72 h. Afterward, the solution was filtered, and the solvent was separated from the extract using a rotary vacuum. The resulting product was stored at a temperature of 4 °C.

2.3. Green synthesis of silver nanoparticles (AgNPs@PCS)

The fabrication of AgNPs was carried out using the following procedure. Initially, an aqueous solution of silver nitrate ($AgNO_3$) was prepared by dissolving 24 mg of silver nitrate in 10 ml of deionized water, resulting in a concentration of 15 mM. The solution was vigorously stirred during the preparation. Simultaneously, an aqueous solution of *Petroselinum crispum* extract was prepared by adding 0.1 g of the extract to 10 ml of deionized water, adjusting the pH to 12. Next, the aqueous solution of *Petroselinum crispum* extract was added to the silver nitrate solution, and the mixture was stirred for 60 min. During this process, the Ag^+ ions were reduced to Ag^0 nanoparticles. The fabricated AgNPs@*PCS* were then subjected to centrifugation at 5000 rpm for 6 min and washed with double distilled water. Finally, the AgNPs@*PCS* were dried in an oven for 24 h. Scheme 1 provides a schematic representation of the biosynthesis of the nanoparticles.

2.3.1. Optimization of fabricated AgNPs@PCS

In order to achieve the optimal shape and size of AgNPs@*PCS*, various parameters were investigated and optimized. The variables studied included silver nitrate concentration, reaction time, and temperature. The objective was to determine the optimum conditions for synthesizing AgNPs@*PCS*. To optimize the concentration, an aqueous solution of *Petroselinum crispum* extract was adjusted to pH 12 using 2 M NaOH, and different concentrations of silver nitrate (5–30 mM) were added to the solution. The sample that exhibited the highest absorption within the range of 300 to 500 nm was considered the best condition. After determining the optimal concentration, time optimization was performed. The green synthesis of AgNPs@*PCS* was carried out at different time intervals (30, 45, 60, 75, 90, 105, and 120 min) while maintaining the optimal concentration. Additionally, temperature optimization was conducted by performing the reaction at different temperatures (25, 55, and 85 °C) while keeping the concentration and reaction time constant. Table 1 provides a summary of the parameters that were investigated for the optimization of AgNPs@*PCS* preparation.

2.4. Antibacterial and antifungal activities of AgNPs@PCS

2.4.1. Minimum inhibitory concentration (MIC) assay

The antifungal and antibacterial properties of AgNPs@*PCS* and *Petroselinum crispum* seeds extract were evaluated using the broth micro-dilution assay in a sterile 96-well microplate. To determine the MIC values, each well of the microplate was filled with 100 µl of Mueller Hinton broth containing varying concentrations of AgNPs@*PCS* and *Petroselinum crispum* seeds extract. Subsequently, 100 µl of a diluted bacterial suspension (equivalent to 0.5 McFarland concentrations, diluted at a ratio of 1/150) was added to each well. The microplate was then shaken for 30 s to ensure thorough mixing and incubated at 37 °C for bacteria and 27 °C for fungi for a period of 24 h. After incubation, the lowest concentration at which no turbidity was observed was considered as the MIC.

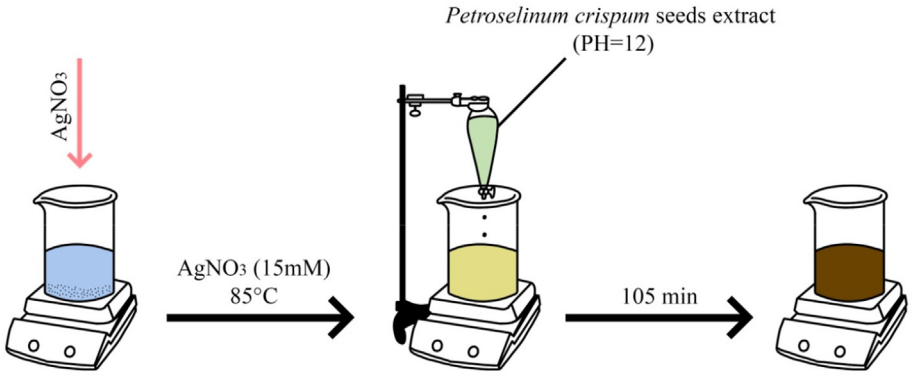

Scheme 1 The stages of formation of silver nanoparticles using *Petroselinum crispum* seed extract.

Table 1 Synthesis of silver nanoparticles using *Petroselinum crispum* seed extract under different conditions such as temperature, time and silver concentration.

Sample no.	Silver concentration (mM)	Time (min)	Temperature (°C)
1	5	60	Room tempt.
2	10	60	Room tempt.
3	15	60	Room tempt.
4	20	60	Room tempt.
5	25	60	Room tempt.
6	30	60	Room tempt.
7	15	30	Room tempt.
8	15	45	Room tempt.
9	15	75	Room tempt.
10	15	90	Room tempt.
11	15	105	Room tempt.
12	15	120	Room tempt.
13	15	105	55
14	15	105	85

2.4.2. Minimum bactericidal concentration (MBC) and minimum fungicidal concentration (MFC) assays

This method was accomplished by taking 10 µl in the wells that no turbidity was observed (MIC concentration and above) and subculturing into Blood Agar. Following the 24-hour incubation, the lowest dilution of AgNPs@*PCS*, *Petroselinum crispum* seeds extract, or vancomycin in which no colonies were observed on the Blood Agar medium was determined as the MBC for bacteria and the MFC for fungi.

2.5. Antioxidant capacity of AgNPs@PCS

The in vitro antioxidant capacity of the AgNPs@*PCS* (sample no. 14) and *Petroselinum crispum* seeds extract was calculated according to the 2,2-Diphenyl-1-Picrylhydrazyl (DPPH) scavenging free radicals method using Zantox kits (Kavosh Arian Azma Co.) (Brand-Williams et al., 1995). In this method, 250 µl of DPPH was added after addition of 10 µl of sample to each well. After shaking for 30 s, plate incubated at room temperature for 20 min. Exposing DPPH radicals to reducing agents or hydrogen donors, leads to change the primary purple to yellow color. These changes can be measured at 517 nm. To calculate the percentage of DPPH radical inhibition, the following formula was utilized (Oryan et al., 2019): Scavenging rate (%) = $(1 - A_s/A_0) \times 100$ (1); Here, A_s represents the absorbance of the sample, while A_0 represents the absorbance of the blank. By substituting the appropriate values into the formula, the percentage of DPPH radical inhibition can be determined.

2.6. Anticancer activity

Anticancer activity was done using the report of Zare-Bidaki and her colleagues (Zare-Bidaki et al., 2022). Human breast cancer cells (MCF-7) were obtained from the Pasteur Institute in Tehran, Iran. The MCF-7 cells were cultured in 75 ml flasks with Dulbecco's Modified Eagle's Medium (DMEM) supplemented with 10% FBS and 1% penicillin/streptomycin. The cell culture was maintained in a 37 °C incubator with 5% CO_2. To evaluate the cytotoxic influence of the fabricated sample (designated as sample no. 14), the MTT assay was performed. Briefly, 10,000 cancer cells were seeded in each well. Following this, the medium in the wells was replaced with fresh medium containing different concentrations of AgNPs (3.25–200 µg/ml). After the incubation period, 10 µl of MTT solution was added to each well. Subsequently, the MTT solution was removed, and DMSO was added, followed by 10 min incubation. The cell viability percentage was calculated using the following formula: Cell viability (%)= (sample absorption/control absorption) × 100 (2). By substituting the appropriate values into equation (2), the cell viability percentage for each sample concentration can be determined.

2.7. Preparation of Vaseline ointment containing AgNPs@PCS

To prepare Vaseline ointment containing AgNPs (sample no. 14), 30 g of pure Vaseline is melted in a bain-marie water bath at 60 °C and 0.3 g of AgNPs@*PCS* were added (1% *w*/*w*). Finally, the prepared ointment was sonicated at 60 °C for 30 min to form uniform.

2.8. In vivo experimental procedure in rat

2.8.1. Burn wound model

Twelve *Wistar* rats (males, 7–9 weeks old, 210 ± 10 g) were chosen and kept in individual cages and all parameters such as diet, temperature, and light were in standard and controlled

for a week before the study. All surgical procedures and experiments conducted in this study were carried out in compliance with the protocols approved by the local Ethics Committee in the Student Research Committee of Birjand University of Medical Sciences. Prior to creating the burn wounds, all animals were anesthetized by intramuscular injection of ketamine (10%, 75 mg/kg body weight) and xylazine (2%, 10 mg/kg body weight). This anesthesia protocol was followed for ensuring the well-being and minimizing any discomfort or pain experienced by the animals during the procedure. Then, the hair of the dorsum of the rats was shaven, and the aluminum bar, which was heated for 20 s in the flame, applied vertically to the skin surface on the back of rats for 10 s without any pressure immediately. Two full-thickness burns, each measuring 10 mm in diameter, were intentionally created on the skin of each rat. The wounds of each rat were divided randomly into four groups as follows:

Group A: The group in which, the wounds were remained untreated (n = 6, negative control group).

Group B: The group in which, the treated wounds by topical use of 1% silver sulfadiazine (n = 6, positive control group).

Group C: The group in which, the treated wounds by topical use of pure Vaseline (n = 6, vehicle control group).

Group D: The group in which, the wounds were treated with 1% *w/w* Vaseline ointment containing sample no. 14 (n = 6, AgNPs@*PCS* group).

Each treatment was applied once a day for 21 days. Two of six rats were euthanized on the days of 7, 14, and 21 post-injuries, and the biopsy specimens were gathered after imaging from the wounded area for analysis. In the Scheme 2, the scheme of the *in vivo* experimental methodology has been shown.

2.8.2. Gross measurements and rate of burn wound closure

Images of the wounds were captured at 0, 7, 14, and 21 days after the wounds were created in order to assess the percentage of wound closure. The captured images were analyzed using Digimizer software version 5.7.2. The percentage of wound closure is used from the following formula:

Wound closure (%) = [(wound area on day 0 - wound area on indicated day)/wound area on day 0] × 100 (3). By substituting the appropriate values into equation (3), the percentage of wound closure for each indicated day can be determined.

2.9. Histopathology

Histological examinations were conducted at three different time points following the injury: 7, 14, and 28 days. To accomplish this, samples of the skin were obtained. All samples were fixed in a 10% neutral buffered formalin solution, dehydrated using various concentrations of ethanol, clarified in xylol, embedded in paraffin, and then sliced into sections measuring 5 μm in thickness. These prepared tissue samples were subjected to staining using hematoxylin and eosin (H&E) and subsequently examined under a standard light microscope. The assessment primarily focused on comparing the degree of epithelialization, infiltration of inflammatory cells, formation of granulation tissue, and the density of blood vessels among the different groups.

2.10. Data analysis

The statistical analysis was conducted using SPSS 19.0 software (Chicago, IL, USA). One-Way ANOVA or Kruskal-Wallis test (for non-parametric variables) was employed, and if the results were found to be significant, Tukey HSD multiple comparisons or Mann-Whitney *U* test (for non-parametric variables) was performed as a post hoc test.

2.11. Characterization

To verify the synthesis of the biofabricated nanoparticles (NPs), various analytical techniques were employed. UV–Vis spectroscopy was performed using a NanoDrop system (BioTek model Epoch, USA) in the wavelength range of 300–500 nm. Fourier infrared spectroscopy (FT-IR) was conducted using a PerkinElmer Spectrum TwoTM IR spectrometer (Model L160000U) in the wave number range of 400–4000 cm^{-1} at room temperature. For further characterization, field emission scanning electron microscopy (FESEM) was performed using a TESCAN BRNO-Mira3 LMU instrument, while transmission electron microscopy (TEM) was performed using a Zeiss-EM10C-100 KV microscope. The crystalline phase and crystallite size of the AgNPs@*PCS* (sample no. 14) were determined using an X-ray diffractometer (Philips PW 1800) with Cu Kα radiation. The particle size and surface charge of the AgNPs@*PCS* (sample no. 14) were assessed using dynamic light-scattering technique (DLS) with a NanoBrook 90Plus instrument (Brookhaven Instruments, model 18051; USA).

3. Results and discussion

3.1. Fabrication of silver nanoparticles (AgNPs@PCS)

UV–Vis spectroscopy was conducted to validate the synthesis of AgNPs, specifically focusing on sample number 14. The process of AgNPs formation can be identified by the alteration in color, transitioning from a pale yellow shade to a deep brown hue, allowing for easy visual observation. The absorbance of different AgNPs samples fabricated under varying conditions was recorded using UV–Vis spectroscopy in the wavelength range of 300–500 nm. The observed color changes in the suspensions resulted in the appearance of a surface plasmon resonance (SPR) absorption band, which can be attributed to the oscillation of free electrons within the metal nanoparticles that resonates with the incident light wave (Ebrahimzadeh et al., 2020; Anandalakshmi et al., 2016). In this study, the reaction parameters that were important for synthesizing the nanoparticles were optimized at different experimental conditions.

3.1.1. Effect of silver nitrate concentration on AgNPs@PCS

The influence of different concentrations of silver nitrate on AgNPs@PCS (sample number 14) was examined using UV/Vis spectra, as depicted in Fig. 1a. It is evident that the molar ratio of silver nitrate concentration is a significant parameter affecting the synthesis of AgNPs. The peaks observed in the UV/Vis spectra indicate that the absorption increases with

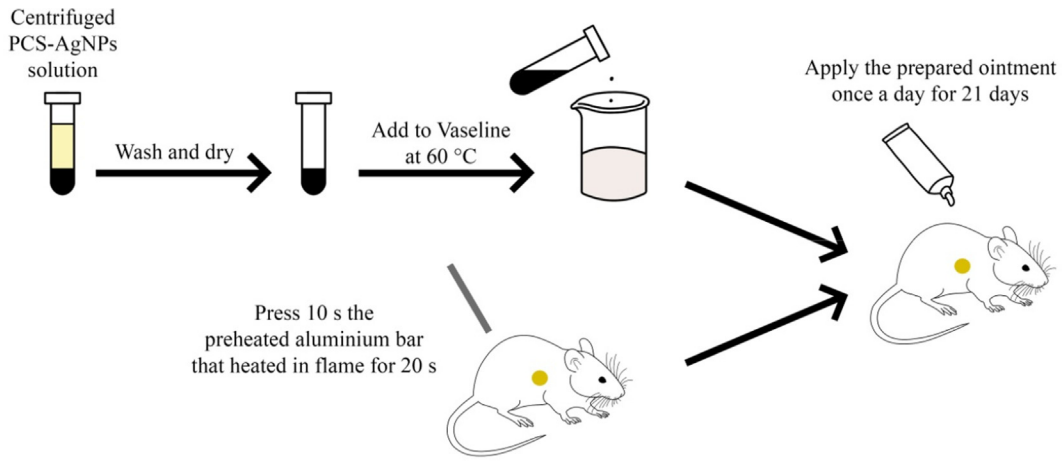

Scheme 2 Scheme of the *in vivo* experimental methodology.

an increase in the concentration of silver nitrate up to 15 mM, after which it starts to decrease. The decrease in the intensity of the absorption band can be attributed to the adhesion and aggregation of nanoparticles (Sharma et al., 2020). Consequently, a concentration of 15 mM was chosen as the optimal concentration due to the maximum absorption associated with it.

3.1.2. Effect of time on AgNPs@PCS

As shown in the UV diagram in Fig. 1b, it is obvious that with increasing in reaction time from 30 to 105 min, the absorption increased that confirmed the best reaction time was about 105 min.

3.1.3. Effect of temperature on AgNPs@PCS

The impact of temperature as a crucial parameter on the nanoparticles synthesis process was investigated. The reaction was conducted under three different temperature conditions: room temperature, 55, and 85 °C. Fig. 1c illustrates that as the temperature was raised from room temperature to 85 °C, the absorption increased significantly. Consequently, the optimum temperature for the synthesis process was determined to be approximately 85 °C. Based on the data presented in Table. 1, sample number 14 was selected as the optimal AgNPs@*PCS* synthesis condition and was utilized for all subsequent experiments.

3.2. XRD analysis

The crystalline structure of the fabricated nanoparticles was assessed through XRD analysis, as depicted in Fig. 2. The XRD results displayed four distinct peaks at 2θ angles of 38.2°, 44.22°, 64.92°, and 77.5°, corresponding to the (1 1 1), (2 0 0), (2 2 0), and (3 1 1) Bragg planes, respectively. These findings indicate the formation of a cubic crystal structure at the core of the AgNPs. Moreover, the obtained results were consistent with the reference data from the Joint Committee on Powder Diffraction Standards (JCPDS 01–087-0717), confirming the high purity of the fabricated nanoparticles as no additional peaks were observed. The outcomes of this study aligned with the findings reported by Ghoshal et al. (Ghoshal and Singh, 2022). The average crystal size of the fabricated nanoparticles was determined using the Debye-Scherr equation ($D = 0.9\lambda/\beta\cos\theta$ (4)), where D represents the average crystal size, λ represents the wavelength, β represents the peak width at half maximum intensity, and θ represents the Bragg angle. According to this calculation, the average crystal size of the fabricated nanoparticles was estimated to be 38.7 nm.

3.3. EDS, FESEM and TEM analysis

The EDS diagram of the fabricated nanoparticles, as illustrated in Fig. 3, exhibited a prominent peak at 3 KeV, primarily associated with AgNPs. Also, small amount of carbon and oxygen were observed in the graph, which is associated to the elements in the extract of *Petroselinum crispum* on the surface of the fabricated nanoparticles. The results of this analysis were in consistent with the results of Rautela *et al.* study (Rautela et al., 2019). FESEM images of fabricated nanoparticles showed the formation of spherical, uniform and homogeneous nanoparticles (Fig. 4). According to these tests, the average size of the fabricated nanoparticles was approximately 30–50 nm. As it is clear, irregular structure that was observed in some areas was related to the aggregation of nanoparticles which can be attributed to the adhesion of the extract on the surface of the NPs. Dinparvar *et al*., reported the fabricated AgNPs using *Cuminum cyminum* L. seed extract and the SEM images of the fabricated nanoparticles showed that the size of the fabricated nanoparticles was about 100 nm. Our data indicated that use of *Petroselinum crispum* extract smaller AgNPs nanoparticles can be fabricated (Dinparvar et al., 2020). Furthermore, TEM spectroscopy was used to obtain the precise size and morphology of the fabricated nanoparticles (Fig. 5). The images clearly showed the spherical and uniform shape of the sample no. 14 with the size around 30–50 nm. The existence of a dark shadow around the fabricated nanoparticles in the TEM images confirmed the placement of *Petroselinum crispum* plant extract on the surface of the fabricated nanoparticles. Ragupathi and his colleagues utilized *Petroselinum crispum* plant extract to synthesize silver nanoparticles (Ragupathi et al., 2016). However, their research resulted in nanoparticles with a rod-like morphology and significant agglomeration. In contrast, our study achieved nanoparticles with more suitable size and morphology, offering an improvement over the previous research.

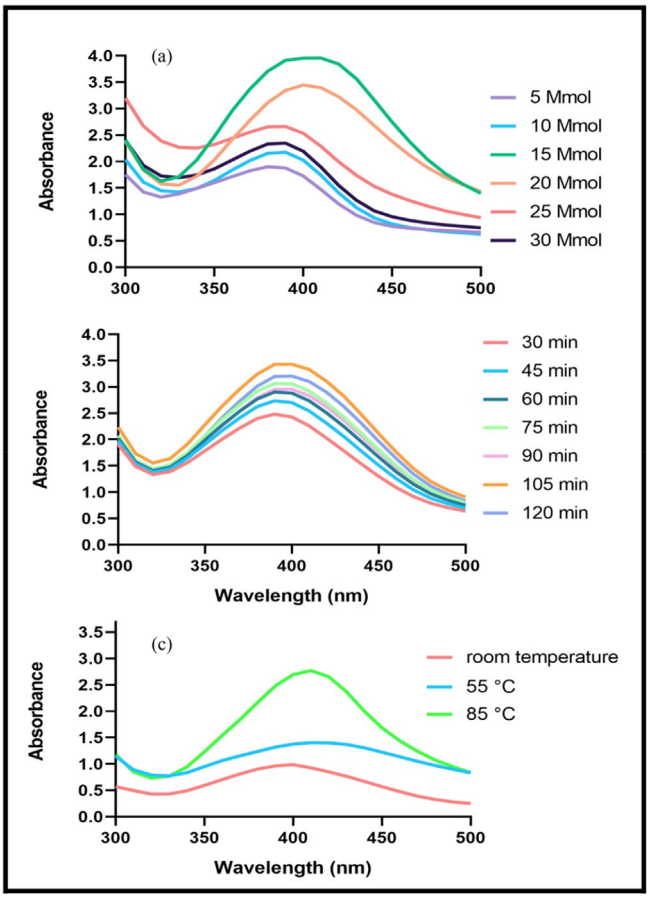

Fig. 1 UV–Vis spectra of the fabricated silver nanoparticles for optimization at various concentration (a), time (b), temperature (c).

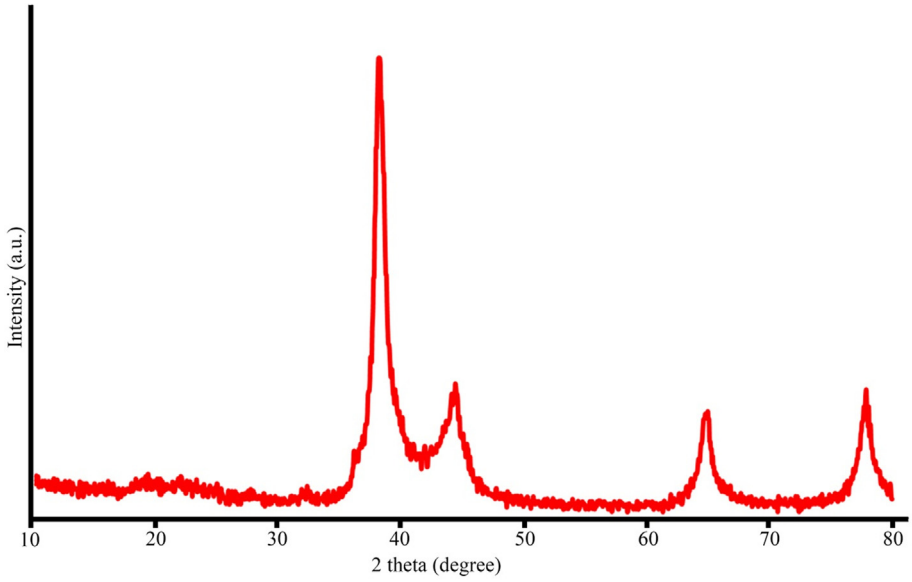

Fig. 2 XRD pattern of AgNPs@*PCS* (sample no. 14).

3.4. DLS and zeta potential analysis

The hydrodynamic diameter of NPs measured by DLS analysis. The hydrodynamic diameter measured the size of the nanoparticles with the various biological components of the extract that are located on the surface of the nanoparticles. For this reason, the size of the NPs in DLS analysis shows a greater value than the results of FESEM and TEM analysis

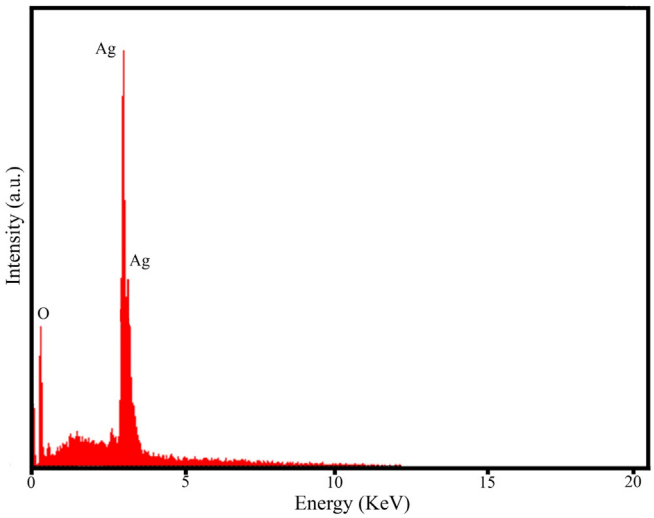

Fig. 3 EDS spectrum of AgNPs@*PCS* (sample no. 14).

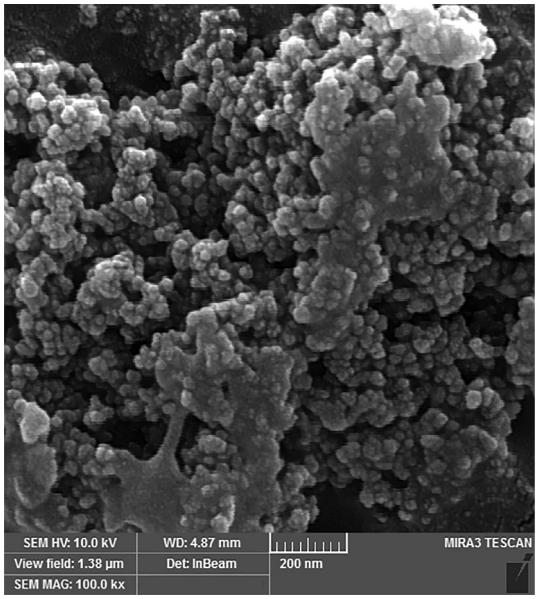

Fig. 4 FESEM images of sample no. 14.

(Kouhbanani et al., 2019). The results of DLS analysis (Fig. 6a) showed the average hydrodynamic diameter of the fabricated nanoparticles about 150 nm. Ravichandran *et al.*, fabricated the AgNPs with the average hydrodynamic diameter about 155.3 nm (Ravichandran et al., 2019). Zeta potential measurement is a method to determine the surface charge of fabricated nanoparticles. The results of zeta potential showed (Fig. 6b) that the fabricated sample no. 14 had a surface charge of –23.2 mV. Negative charge of the fabricated nanoparticles indicated the presence of extract compounds on the surface (Ravichandran et al., 2019). Other benefit of using plants extract as a capping agent is due to the charge on the surface of nanoparticles which cause the repulsion between particles and then, high stability of the suspension obtained. The high surface charge of sample no. 14 indicated the high stability of the fabricated nanoparticles. Sharma *et al.* reported the negative charge on the surface of fabricated sample no. 14 that was the same result with our study, (Sharma et al., 2018).

3.5. FT-IR

The formation of nanoparticles and the involvement of functional groups were examined through FT-IR analysis. The FT-IR spectrum of *Petroselinum crispum* extract revealed absorption bands at specific wavenumbers: 3384.1, 2912.6, 1712.3, 1237.7, 1055.2, and 814.5 cm^{-1} (Fig. 7). The absorption peak at 3384.1 cm^{-1} indicated strong stretching vibrations of the O—H functional group in alcoholic and phenolic groups (Isaac et al., 2013). The peak observed at 2912.6 cm^{-1} was attributed to the stretching of the C—H group in alkenes (Dhand et al., 2016). The peak at 1712.3 cm^{-1} could be associated with the stretching or bending of the C═O group present in amides (Mahadevan et al., 2017). The peak at 1237.7 cm^{-1} was related to the C—O stretching of the ester group (Chinnasamy et al., 2019). The observed peak at 1055.2 cm^{-1} indicated the C═O stretching of the alcoholic group (Chinnasamy et al., 2019). The absorption peak at 814.5 cm^{-1} was related to the C—H bending of the alkynes group (Paulkumar et al., 2014). Fig. 7 depicted the fabricated AgNPs using *Petroselinum crispum* extract. It can be observed that the FT-IR spectrum of the fabricated nanoparticles was similar to the FT-IR spectrum of *Petroselinum crispum* extract, albeit with lower displacement and intensity. This similarity indicates the influence of functional groups present in *Petroselinum crispum* extract in reducing Ag^{+} ions to Ag^{0} nanoparticles (Khodadadi et al., 2021).

3.6. Antibacterial and antifungal activity

The antibacterial properties of AgNPs@*PCS* (sample number 14) were evaluated against both gram-negative (*Escherichia coli* and *Klebsiella pneumoniae*) and gram-positive bacteria (*Staphylococcus aureus*, *Streptococcus mutans*, *Streptococcus mitis* and *Enterococcus faecalis*), as presented in Table. 2. It was observed that the effectiveness of AgNPs@*PCS* against gram-negative bacteria was higher compared to gram-positive

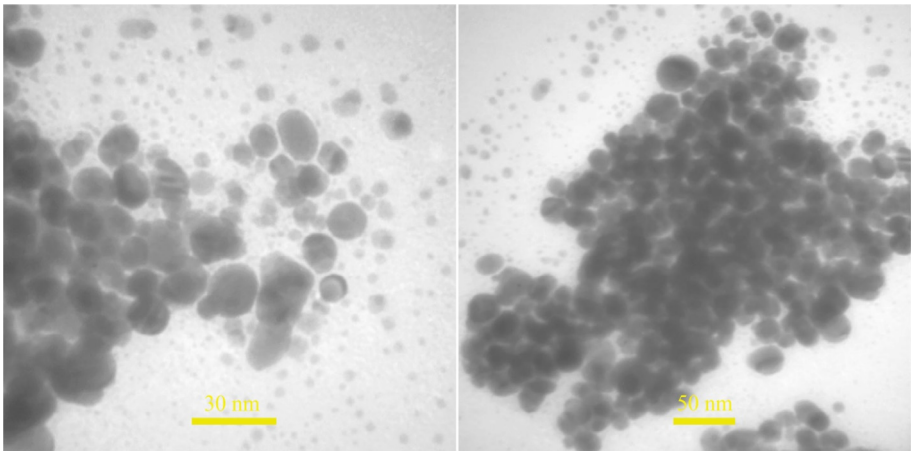

Fig. 5 TEM images of sample no. 14.

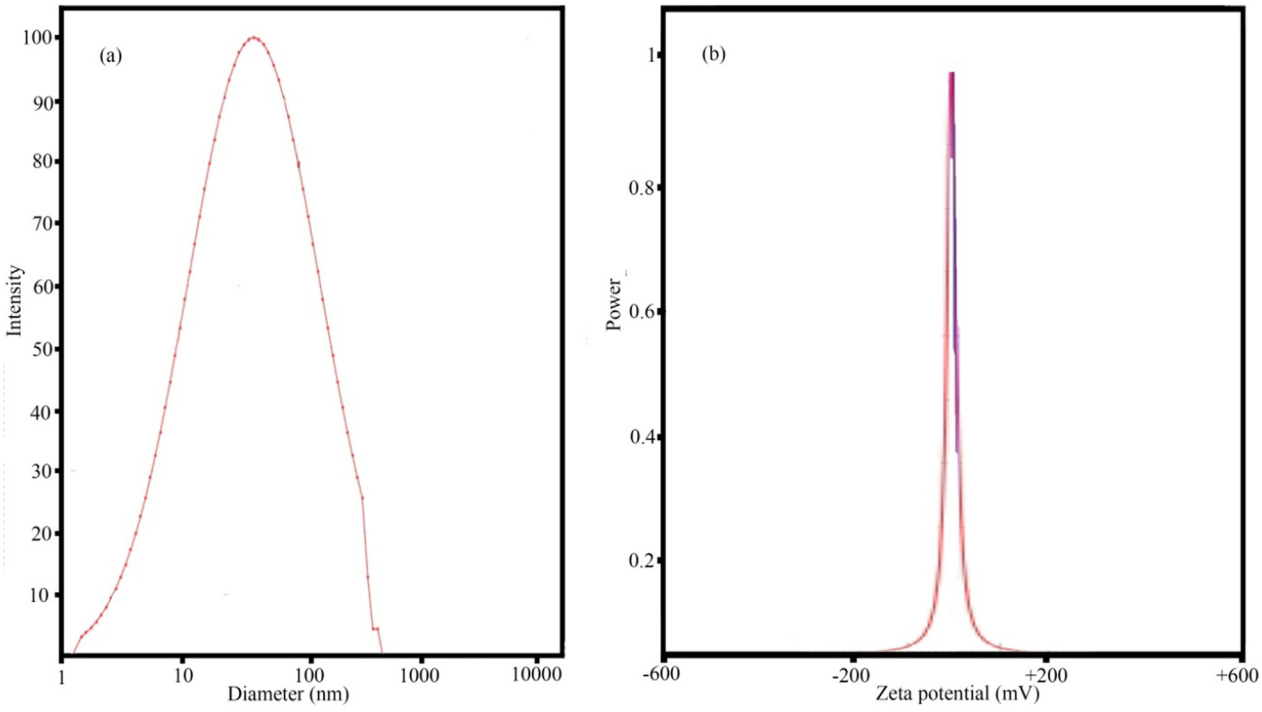

Fig. 6 DLS and zeta potential analysis of images of sample no. 14.

bacteria, consistent with the well-known trend in which silver nanoparticles exhibit greater antimicrobial activity against gram-negative strains. *Escherichia coli* showed the greatest effect of AgNPs@*PCS* (sample no. 14) on gram-negative bacteria with MIC about 31.25 µg/ml, and *Streptococcus mitis* and *Enterococcus faecalis* showed the lower effect on gram-positive bacteria with MIC around 250 µg/ml. The difference between gram-positive and gram-negative bacteria is the existence of a thicker peptidoglycan layer in gram-positive cell wall and maybe the main reason influencing the more effect of AgNPs@*PCS* on gram-negative bacteria (Monedeiro et al., 2019). Furthermore, gram-negative bacteria have a lipopolysaccharide layer that has a positive charge, but AgNPs@*PCS* has a negative surface charge, which causes more accumulation of nanoparticles on the surface of gram-negative bacteria (Sharifi-Rad et al., 2020). AgNPs fabricated in Behravan *et al*. study using *Berberis vulgaris* aqueous extract showed more antibacterial effects against gram-negative bacteria same as in our study (Behravan et al., 2019). Haq Khan and his colleagues successfully produced silver nanoparticles using an extract derived from the *Petroselinum crispum* plant. The antibacterial activity of these nanoparticles was evaluated against *Escherichia coli* and *Staphylococcus aureus* bacteria, and the results indicated that the MIC for *Escherichia coli* was 235 µl/ml, while for *Staphylococcus aureus*, it was 120 µl/ml. Notably, our antibacterial activity was more effective against *Escherichia coli* (MIC value of 31.25 µl/ml) compared to their study (Khan et al., 2020). This can be attributed to achieving the optimal conditions for nanoparticle synthesis, ensuring the nanoparticles possessed the appropriate

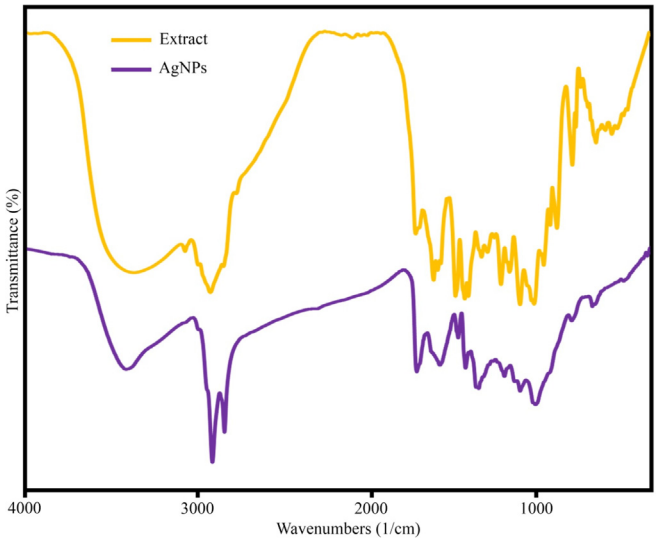

Fig. 7 FT-IR of sample no. 14 and extract.

Table 2 MIC and MBC values (μg/ml) of AgNPs@*PCS* (sample no. 14).

Microorganism	AgNPs@*PCS*		*Petroselinum crispum*	
	MIC (μg/ml)	MBC (μg/ml)	MIC (μg/ml)	MBC (μg/ml)
Escherichia coli	31.25	62.5	> 4000	> 4000
Klebsiella pneumoniae	62.5	62.5	> 4000	> 4000
Staphylococcus aureus	125	250	> 4000	> 4000
Enterococcus faecalis	250	500	> 4000	> 4000
Streptococcus mutans	250	250	> 4000	> 4000
Streptococcus mitis	250	500	> 4000	> 4000

size and morphology. In this study, the antifungal effect of AgNPs@*PCS* against *Candida albicans* strain was investigated. The results showed (Table. 3) that the strong effect of fabricated nanoparticles on antifungal with the MIC = 15.62 μg/ml. Rizwana and colleagues, reported the fabricated AgNPs that had significant antifungal properties (Rizwana et al., 2021). Studies claimed that shape and size of the nanoparticles directly affect the antimicrobial activity, so that the smaller size of the NPs and the higher the surface-to-volume ratio, shows the stronger antimicrobial activity (Mitiku and Yilma, 2018). One of the possible mechanisms of the antimicrobial effects of silver nanoparticles is nanoparticles binding to the bacterial cell wall and the creation of free radicals. Then, disturbance in the permeability of the membrane and the entry of silver ions into the bacteria occur (Pirtarighat et al., 2019). Ag^{+} ions disrupt the function of the bacteria by binding to phosphorus and sulfur in DNA, RNA or proteins and eventually destroy it (Ahmad et al., 2022, 2022).

Table 3 MIC and MFC of AgNPs@*PCS* against *C. albicans* (sample no. 14).

Microorganism	AgNPs@*PCS*	
	MIC (μg/ml)	MFC (μg/ml)
C. albicans	15.62	62.5

3.7. Analysis of total antioxidant properties (TAC)

Free radicals are cell metabolisms that have one or more unpaired electrons in their outer electron orbit. The presence of these unpaired electrons makes them highly reactive that make instability by transferring the electron and damaging the cell and eventually cell death happen, so-called oxidative stress (Gonca et al., 2021). In order to prevent this damage, cells have antioxidant molecules that neutralize them by giving electrons to free radicals and thus prevent damage to cells (Liguori et al., 2018). Oxidative stress causes various diseases such as Alzheimer's, cancer, arteriosclerosis, and chronic lung obstruction. The use of antioxidants can significantly reduce the risks of oxidative stress (Forman and Zhang, 2021). The DPPH scavenging free radicals was employed to examine the antioxidant capabilities of AgNPs@*PCS* and *Petroselinum crispum*. The results of examining the antioxidant properties of AgNPs@*PCS* and *Petroselinum crispum* in Fig. 8 are remarkable. As can be seen, *Petroselinum crispum* extract has been able to increase the percentage of DPPH radical inhibition from 11 to 83% by increasing the concentration from 3.12 to 25 mg/ml. Also, the results revealed that the use of *Petroselinum crispum* extract for the synthesis of AgNPs

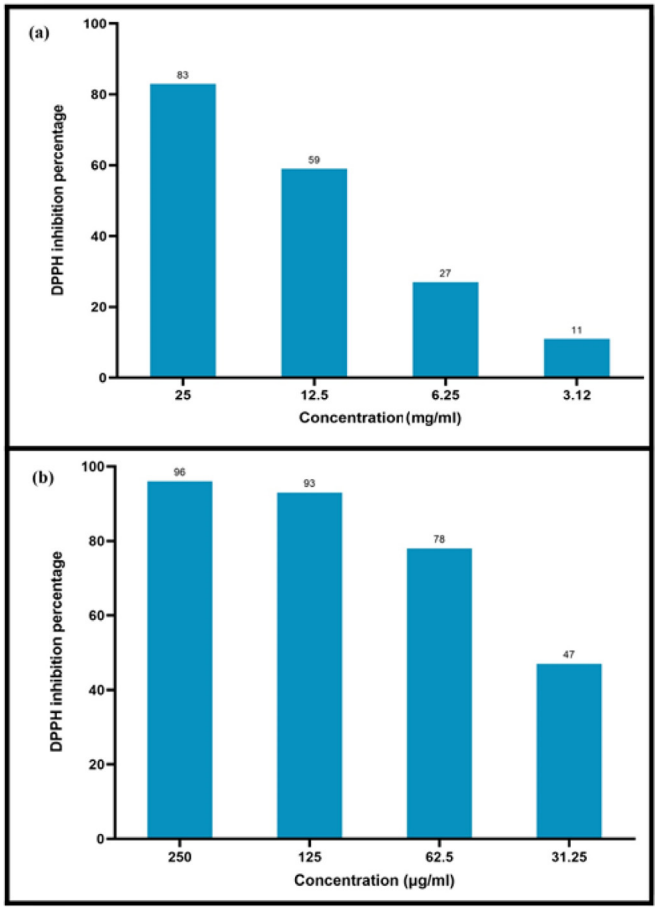

Fig. 8 DPPH inhibition percentage at different concentrations of AgNPs@*PCS* (sample no. 14) (a) and PCS extract (b).

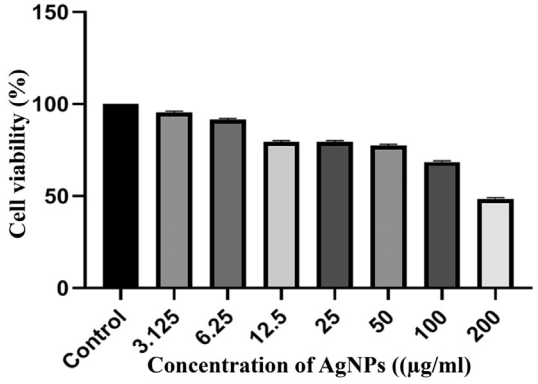

Fig. 9 The results of the MTT assay in MCF-7 Cell treated with AgNPs after 24 h. Results were reported as survival percentage compared to control samples.

significantly increased the antioxidant capacity of AgNPs, therefore the AgNPs@*PCS* could inhibit free radicals about 47% at the 31.25 µg/ml concentration. Also, the percentage of inhibition increasing with the increasing in concentration so that at a concentration of 250 µg/ml, it inhibited 96% of DPPH. The results of the present study are similar to previous studies (Khorrami et al., 2018). Lalitha *et al.*, published the fabricated AgNPs by *Azhadirachta indica* extract that inhibited DPPH radical about 48% at 250 µg/ml concentration, which showed a lower antioxidant activity compared to the nanoparticles fabricated in our study (Lalitha et al., 2013). As a result, AgNPs@*PCS* can be considered as nanoparticles with high antioxidant capacity.

3.8. Anticancer activity

The cytotoxicity of the prepared nanoparticles was assessed using the MTT assay at various concentrations of AgNPs (3.25, 6.25, 12.5, 25, 50, 100, 200 µg/ml) on MCF-7 cell lines, as shown in Fig. 9. It can be observed that the viability of cancer cells decreased as the concentration of AgNPs increased. At the lowest concentration, 100% cell viability was observed, while at concentrations of 100 µg/ml and 200 µg/ml, cell viability decreased to approximately 69% and 49%, respectively. In this study, the IC50 value of the AgNPs was determined to be 200 µg/ml. In a study conducted by Farah et al. (Farah et al., 2016), IC50 value of 217 µg/ml was found for AgNPs fabricated using *A. obesum* leaves extract against MCF-7 cells. On the other hand, Moteriya et al. (Moteriya and Chanda, 2020) fabricated AgNPs using leaf extract of *Caesalpinia pulcherrima* for the treatment of human breast cancer cells (MCF-7), and the IC50 value was reported to be approximately 70 µg/ml after 24 h.

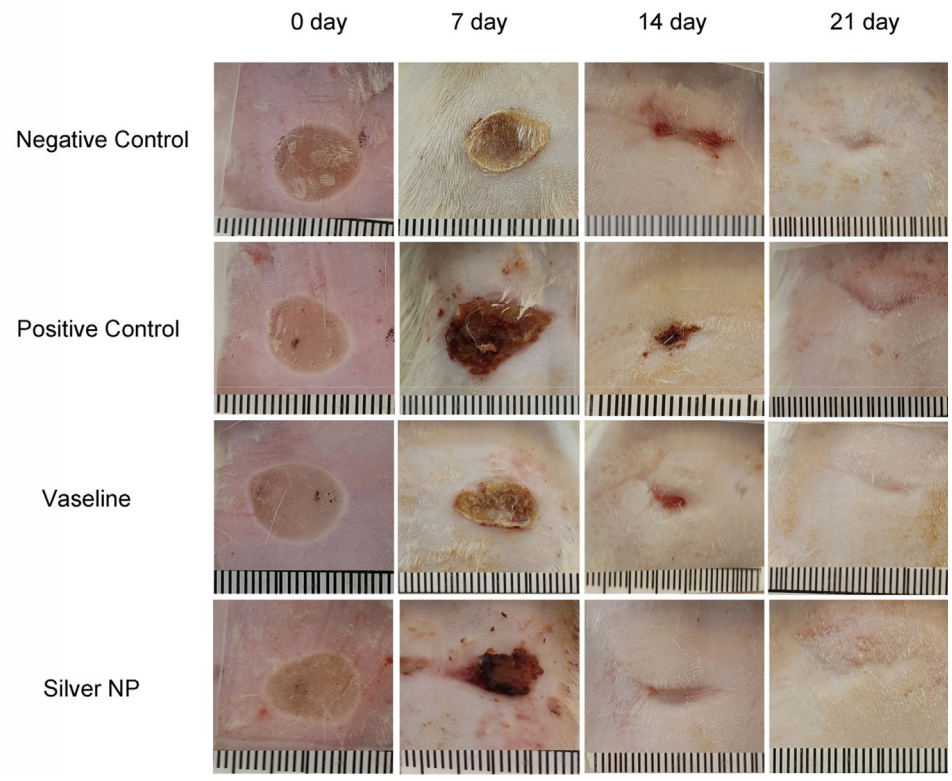

Fig. 10 Effect of AgNPs@*PCS* group (Silver NP), pure Vaseline (Vaseline), silver sulfadiazine (Positive control) and Negative control on the wound closure rate in rats.

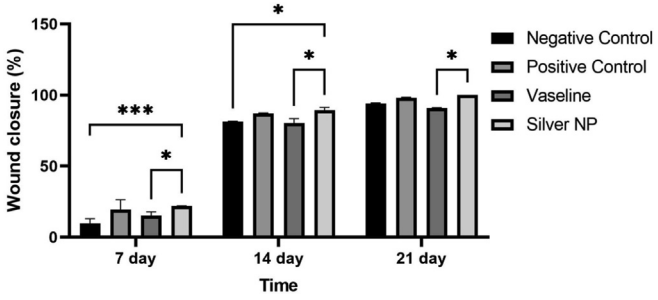

Fig. 11 Percentage of wound closure at 7, 14 and 21 days post-injury (mean ± SD) ($p < 0.001$ ***, $p < 0.01$ **, $p < 0.05$ *).

3.9. Evaluation of wound closure percentage

The rate of wound closure was assessed by calculating the area of the unclosed wound in Fig. 10. The data revealed a significant increase in the percentage of wound closure in the nanoparticles group compared to both the negative control group and the Vaseline group after 7 and 14 days (Fig. 11). By the 21st day, the wounds in the nanoparticles group were completely closed, and a significant difference was observed compared to the Vaseline group at this time point. In a related study, Oryan et al. {Oryan, 2018 #79} (Oryan et al., 2018) investigated the therapeutic effect of AgNPs coated with chitosan. Their results demonstrated that the group treated with a high dose of nanoparticles exhibited significantly higher wound closure percentages than the control groups on the seventh day after injury. These findings indicate the promising wound healing properties of AgNPs, especially in combination with chitosan or other wound healing agents, which could potentially accelerate the wound closure process and promote better recovery. Further investigation showed that in both treatment groups using high and low doses of AgNPs coated with chitosan, the percentage of wound closure were in agreement with the results obtained in our study. Also, Tian & co-workers followed the appearance of healed wounds, and it was found that the healed wounds using AgNPs group were similar to normal skin. This study showed that wounds healing in the group treated with AgNPs was about 60%, while it was about 40% in the control groups (Tian et al., 2007). The results of our study and previous studies showed that the use of AgNPs plays a significant role in accelerating the healing of

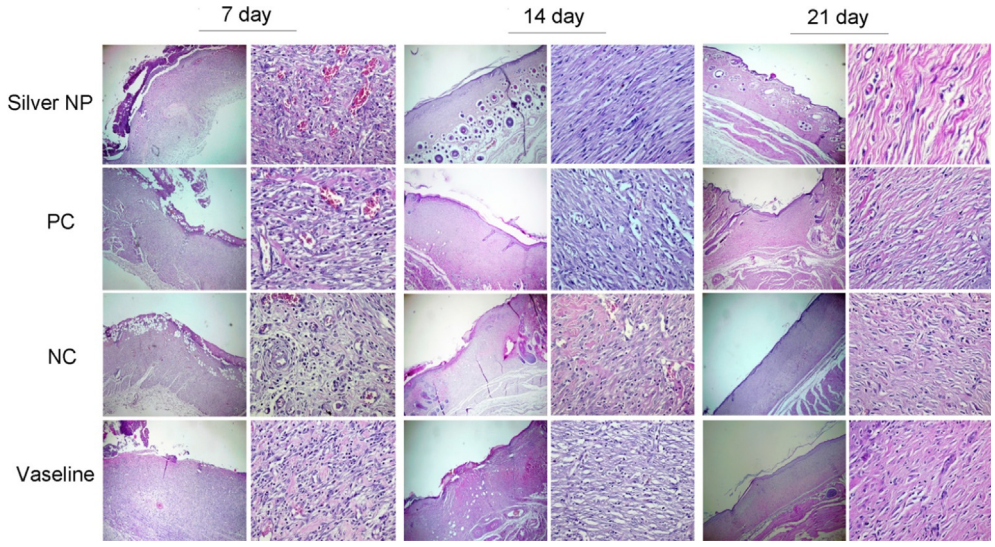

Fig. 12 Histopathology of wounds on the 7th, 14th, and 21th days after injury (hematoxylin and eosin, ×40 and × 400).

skin wounds. Also, in addition to accelerating the formation of granulation tissue and re-epithelialization, AgNPs play a role in reducing the size of the wound more rapidly and forming the normal appearance of the skin.

3.10. Histopathological assays

Histological analysis of the wounds on days 7, 14, and 21 was conducted and presented in Fig. 12. The results indicated that re-epithelialization was completed after 14 days in the group treated with nanoparticles, and the damaged region was entirely covered with a thick and mature epidermis. Notably, the number of blood vessels in the group treated with nanoparticles ointment did not show a significant difference compared to the other groups ($p > 0.05$). Furthermore, after 7 days of treatment with AgNPs@*PCS* ointment (sample number 14), a significant decrease in the number of inflammatory cells was observed compared to the group treated with Vaseline ($p < 0.05$), as shown in Fig. 13. Similarly, the results indicated a significant decrease in the number of inflammatory cells in the nanoparticles ointment-treated group compared to the negative control group and Vaseline after 14 days of treatment ($p < 0.05$) (Fig. 13). Interestingly, wounds treated with AgNPs@*PCS* ointment exhibited a significant increase in the number of fibroblasts and fibrocytes after 7 and 14 days of treatment compared to the other groups ($p < 0.05$) (Fig. 13). However, after 21 days, the group treated with AgNPs@*PCS* ointment showed a significant decrease in the number of fibroblasts and fibrocytes compared to the other groups ($p < 0.05$) (Fig. 13). The results obtained after 21 days of treatment showed the regular structure of connective tissue bundles in the dermis in the group treated with AgNPs@*PCS* ointment. Generally, the group treated with AgNPs@*PCS* ointment showed a decrease in the number of inflammatory cells and increase in fibroblasts and fibrocytes, and regular organization of collagen fibers compared to Vaseline and negative control groups. Results support our hypothesis that the use of AgNPs@*PCS* ointment can be used as a favorable option for the reconstruction of damaged areas and wounds. Based on the results obtained by histopathological evaluations, AgNPs@*PCS* ointment led to a significant reduction of inflammatory cells. Also, data confirmed the improvement and acceleration of granulation tissue formation and re-epithelialization by AgNPs@*PCS* ointment. The histopathology results of our study showed that Vaseline ointment containing AgNPs@*PCS* prevented inflammation in the wound area and increased the number of fibroblast cell production and migration that lead to the acceleration of wound healing. Moreover, prevention from infection at the wound site is the other benefit of AgNPs@*PCS* (sample no. 14) due to its potential antimicrobial property. According to the study conducted by Tian & co-workers, the most benefit of AgNPs in wound healing process in mice was to increase the speed of wound healing. In addition, green fabricated AgNPs have the ability to prevent wound infection due to their antibacterial effect, which prevents secondary damage into wounds during the healing period. On the other hand, the ability to reduce wound inflammation by reducing the infiltration of mast cells and lymphocytes and modulating fibrogenic cytokines such as IL-6 showed satisfactory results. The results of this study demonstrated that the use of silver nanoparticles in burn wounds can be a new and effective treatment to achieve scar-free wound healing at the bedside (Tian et al., 2007). Also, in a study by Liu & co-workers, it was shown that AgNPs can differentiate fibroblasts into myofibroblasts, thus wound contraction can be promoted. Moreover, the restorative nature of AgNPs was shown by increasing the production of keratinocytes and their movement into the wound site (Liu et al., 2010). Also, Lakkim & co-workers revealed that the use of AgNPs in the treatment of burn wounds prevented microbial growth, bleeding, or pus formation during treatment. Also, this study showed that the use of Vaseline ointment containing AgNPs accelerated the reduction of wound size, which was due to the anti-microbial effect of green fabricated AgNPs around the wound area (Lakkim et al., 2020).

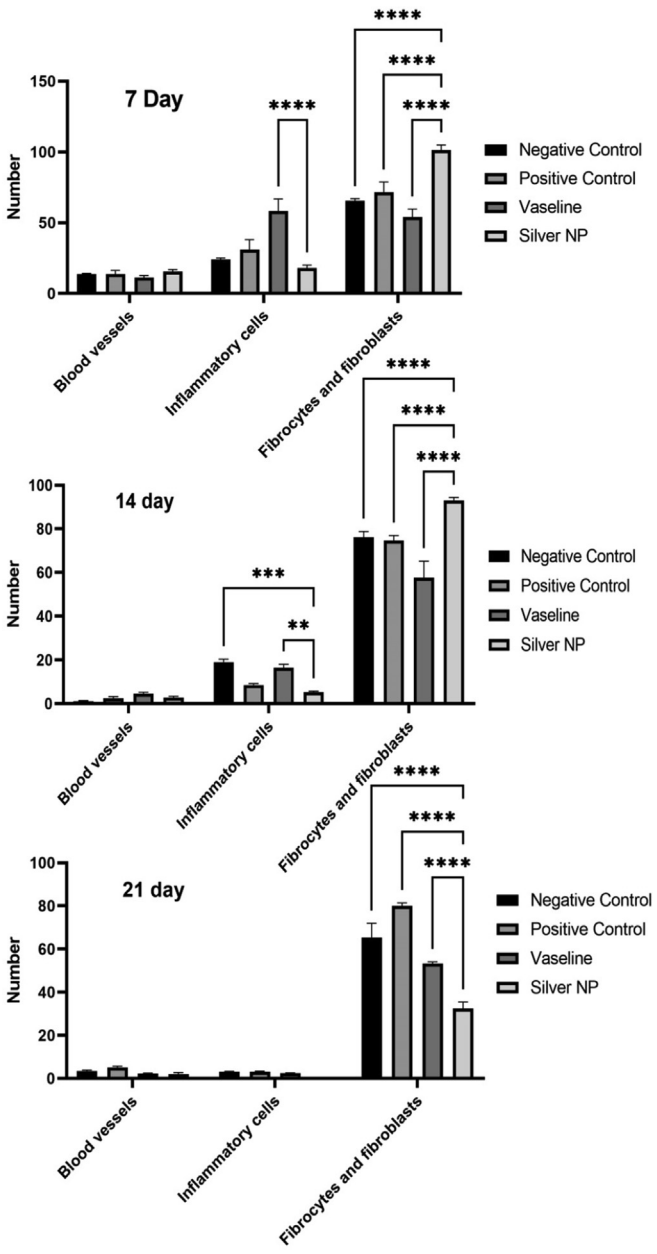

Fig. 13 histological analysis of wounds after 7, 14, and 21 days of injuring ($p < 0.001$ ****, $p < 0.005$ ***, $p < 0.01$ **, $p < 0.05$ *).

4. Conclusion

In conclusion, this research demonstrates the successful synthesis of silver nanoparticles using *Petroselinum crispum* seed extract as both reducing and capping agents, employing a simple, environmentally friendly, and accessible approach. The study highlights the significant impact of silver salt concentration, temperature, and reaction time on the size and concentration of the fabricated nanoparticles, as revealed by UV–Vis analysis. The fabricated silver nanoparticles exhibited potent antibacterial and antifungal activity against various bacteria, as well as *Candida albicans* fungi. Additionally, their impressive antioxidant capacity, demonstrated by inhibiting 96% of DPPH radicals at a concentration of 250 μg/ml, highlights their potential therapeutic applications. Furthermore, the study revealed promising anticancer activity on the MCF-7 cell line, suggesting the possible use of these nanoparticles in cancer treatment. The investigation of wound healing properties demonstrated that Vaseline ointment containing the fabricated AgNPs effectively promoted wound closure and exhibited notable wound healing activity. These findings underscore the multifaceted potential of Petroselinum crispum seed extract-mediated silver nanoparticles in various biomedical applications.

Acknowledgements

In this investigation, the entire procedures were conducted according to the Helsinki Declaration and ethical standards of the institutional research committee. The ethics code was taken from Birjand University of Medical Sciences (IR.BUMS.REC.1401.045).

References

Abbasi, N., Ghaneialvar, H., Moradi, R., Zangeneh, M.M., Zangeneh, A., 2021. Formulation and characterization of a novel cutaneous wound healing ointment by silver nanoparticles containing Citrus lemon leaf: a chemobiological study. Arab. J. Chem. 14, 103246.

Ahmad, N., Fozia, M., Jabeen, Z.U., Haq, I., Ahmad, A., Wahab, Z. U., Islam, R., Ullah, A., Bari, M.M., Abdel-Daim, F.M., El-Demerdash, M.Y.K., 2022,. Green fabrication of silver nanoparticles using *Euphorbia serpens Kunth* aqueous extract, their characterization, and investigation of its *in vitro* antioxidative, antimicrobial, insecticidal, and cytotoxic activities. Biomed Res. Int. 5562849

Ahmad, S., Munir, S., Zeb, N., Ullah, A., Khan, B., Ali, J., Bilal, M., Omer, M., Alamzeb, M., Salman, S.M., Ali, S., 2019. Green nanotechnology: a review on green synthesis of silver nanoparticles - an ecofriendly approach. Int. J. Nanomed. 14, 5087–5107.

Anandalakshmi, K., Venugobal, J., Ramasamy, V., 2016. Characterization of silver nanoparticles by green synthesis method using Pedalium murex leaf extract and their antibacterial activity. Appl. Nanosci. 6, 399–408.

Arassu, R.T., Nambikkairaj, B., Ramya, D., 2018. Pelargonium graveolens plant leaf essential oil mediated green synthesis of Silver Nano particles and its antifungal activity against human pathogenic fungi. J. Pharm. Phytochem. 7, 1778–1784.

Behravan, M., Hossein Panahi, A., Naghizadeh, A., Ziaee, M., Mahdavi, R., Mirzapour, A., 2019. Facile green synthesis of silver nanoparticles using Berberis vulgaris leaf and root aqueous extract and its antibacterial activity. Int. J. Biol. Macromol. 124, 148–154.

Brand-Williams, W., Cuvelier, M.E., Berset, C., 1995. Use of a free radical method to evaluate antioxidant activity. LWT Food Sci. Technol. 28, 25–30.

Burdușel, A.C., Gherasim, O., Grumezescu, A.M., Mogoantă, L., Ficai, A., Andronescu, E., 2018. Biomedical applications of silver nanoparticles: an up-to-date overview. Nanomaterials (Basel) 8.

Chinnasamy, G., Chandrasekharan, S., Bhatnagar, S., 2019. Biosynthesis of silver nanoparticles from melia azedarach: enhancement of antibacterial, wound healing, antidiabetic and antioxidant activities. Int. J. Nanomed. 14, 9823–9836.

de Menezes Epifanio, N.M., Cavalcanti, L.R.I., Dos Santos, K.F., Duarte, P.S.C., Kachlicki, P., Ożarowski, M., Riger, C.J., de Almeida Chaves, D.S., 2020. Chemical characterization and in vivo antioxidant activity of parsley (Petroselinum crispum) aqueous extract. Food Funct. 11, 5346–5356.

Dhand, V., Soumya, L., Bharadwaj, S., Chakra, S., Bhatt, D., Sreedhar, B., 2016. Green synthesis of silver nanoparticles using Coffea arabica seed extract and its antibacterial activity. Mater. Sci. Eng. C 58, 36–43.

Dinparvar, S., Bagirova, M., Allahverdiyev, A.M., Abamor, E.S., Safarov, T., Aydogdu, M., Aktas, D., 2020. A nanotechnology-based new approach in the treatment of breast cancer: biosynthesized silver nanoparticles using Cuminum cyminum L. seed extract. J. Photochem. Photobiol. B Biol. 208, 111902.

Doan Thi, T.U., Nguyen, T.T., Thi, Y.D., Ta Thi, K.H., Phan, B.T., Pham, K.N., 2020. Green synthesis of ZnO nanoparticles using orange fruit peel extract for antibacterial activities. RSC Adv. 10, 23899–23907.

Ebrahimzadeh, M.A., Naghizadeh, A., Amiri, O., Shirzadi-Ahodashti, M., Mortazavi-Derazkola, S., 2020. Green and facile synthesis of Ag nanoparticles using Crataegus pentagyna fruit extract (CP-AgNPs) for organic pollution dyes degradation and antibacterial application. Bioorg. Chem. 94, 103425.

El-Borady, O.M., Ayat, M.S., Shabrawy, M.A., Millet, P., 2020. Green synthesis of gold nanoparticles using Parsley leaves extract and their applications as an alternative catalytic, antioxidant, anticancer, and antibacterial agents. Adv. Powder Technol. 31, 4390–4400.

Farah, M.A., Ali, M.A., Chen, S.M., Li, Y., Al-Hemaid, F.M., Abou-Tarboush, F.M., Al-Anazi, K.M., Lee, J., 2016. Silver nanoparticles synthesized from Adenium obesum leaf extract induced DNA damage, apoptosis and autophagy via generation of reactive oxygen species. Colloids Surf. B Biointerfaces 141, 158–169.

Forman, H.J., Zhang, H., 2021. Targeting oxidative stress in disease: promise and limitations of antioxidant therapy. Nat. Rev. Drug Discov. 20, 689–709.

Ghoshal, G., Singh, M., 2022. Characterization of silver nano-particles synthesized using fenugreek leave extract and its antibacterial activity. Mater. Sci. Energy Technol. 5, 22–29.

Gonca, S., Arslan, H., Isik, Z., Özdemir, S., Dizge, N., 2021. The surface modification of ultrafiltration membrane with silver nanoparticles using Verbascum thapsus leaf extract using green synthesis phenomena. Surf. Interfaces 26, 101291.

Hasan, M., Altaf, M., Zafar, A., Hassan, S.G., Ali, Z., Mustafa, G., Munawar, T., Saif, M.S., Tariq, T., Iqbal, F., Khan, M.W., Mahmood, A., Mahmood, N., Shu, X., 2021. Bioinspired synthesis of zinc oxide nano-flowers: A surface enhanced antibacterial and harvesting efficiency. Mater. Sci. Eng. C 119, 111280.

Hussain, I., Singh, N.B., Singh, A., Singh, H., Singh, S.C., 2016. Green synthesis of nanoparticles and its potential application. Biotechnol. Lett 38, 545–560.

Isaac, R.S.R., Sakthivel, G., Murthy, C., 2013. Green synthesis of gold and silver nanoparticles using *Averrhoa bilimbi* fruit extract. J. Nanotechnol. 2013, 906592.

Jadoun, S., Arif, R., Jangid, N.K., Meena, R.K., 2021. Green synthesis of nanoparticles using plant extracts: a review. Environ. Chem. Lett. 19, 355–374.

Jayarambabu, N., Akshaykranth, A., Venkatappa Rao, T., Venkateswara Rao, K., Rakesh Kumar, R., 2020. Green synthesis of Cu nanoparticles using Curcuma longa extract and their application in antimicrobial activity. Mater. Lett. 259, 126813.

Khan, Z.U.H., Shah, N.S., Iqbal, J., Khan, A.U., Imran, M., Alshehri, S.M., Muhammad, N., Sayed, M., Ahmad, N., Kousar, A., Ashfaq, M., Howari, F., Tahir, K., 2020. Biomedical and photocatalytic applications of biosynthesized silver nanoparticles: Ecotoxicology study of brilliant green dye and its mechanistic degradation pathways. J. Mol. Liq. 319, 114114.

Khodadadi, S., Mahdinezhad, N., Fazeli-Nasab, B., Heidari, M.J., Fakheri, B., Miri, A., 2021. Investigating the possibility of green synthesis of silver nanoparticles using vaccinium arctostaphlyos extract and evaluating its antibacterial properties. Biomed Res. Int. 2021, 5572252.

Khorrami, S., Zarrabi, A., Khaleghi, M., Danaei, M., Mozafari, M.R., 2018. Selective cytotoxicity of green synthesized silver nanoparticles against the MCF-7 tumor cell line and their enhanced antioxidant and antimicrobial properties. Int. J. Nanomed. 13, 8013–8024.

Kouhbanani, M.A.J., Beheshtkhoo, N., Nasirmoghadas, P., Yazdanpanah, S., Zomorodianc, K., Taghizadeh, S., Amani, A.M., 2019. Green synthesis of spherical silver nanoparticles using Ducrosia anethifolia aqueous extract and its antibacterial activity. J. Environ. Treatment Techniques 7, 461–466.

Lakkim, V., Reddy, M.C., Pallavali, R.R., Reddy, K.R., Reddy, C.V., Inamuddin, A.L., Bilgrami, D.L., 2020. Green synthesis of silver nanoparticles and evaluation of their antibacterial activity against multidrug-resistant bacteria and wound healing efficacy using a murine model. Antibiotics (Basel) 9.

Lalegani, Z., Ebrahimi, S.A.S., Hamawandi, B., La Spada, L., Toprak, M.S., 2020. Modeling, design, and synthesis of gram-scale monodispersed silver nanoparticles using microwave-assisted polyol process for metamaterial applications. Opt. Mater. 108, 110381.

Lalitha, A., Subbaiya, R., Ponmurugan, P., 2013. Green synthesis of silver nanoparticles from leaf extract Azhadirachta indica and to study its anti-bacterial and antioxidant property. Int. J. Curr. Microbiol. App. Sci. 2, 228–235.

Liguori, I., Russo, G., Curcio, F., Bulli, G., Aran, L., Della-Morte, D., Gargiulo, G., Testa, G., Cacciatore, F., Bonaduce, D., Abete, P., 2018. Oxidative stress, aging, and diseases. Clin. Interv. Aging 13, 757–772.

Lin, S.K., Cheng, W.T., 2020. Fabrication and characterization of colloidal silver nanoparticle via photochemical synthesis. Mater. Lett. 261, 127077.

Liu, X., Lee, P.Y., Ho, C.M., Lui, V.C., Chen, Y., Che, C.M., Tam, P. K., Wong, K.K., 2010. Silver nanoparticles mediate differential responses in keratinocytes and fibroblasts during skin wound healing. ChemMedChem 5, 468–475.

Mahadevan, S., Vijayakumar, S., Arulmozhi, P., 2017. Green synthesis of silver nano particles from Atalantia monophylla (L) Correa leaf extract, their antimicrobial activity and sensing capability of H(2)O (2). Microb. Pathog. 113, 445–450.

Mitiku, A.A., Yilma, B., 2018. A review on green synthesis and antibacterial activity of silver nanoparticles. Int. J. Pharm. Sci. Rev. Res 46, 52–57.

Mohammadzadeh, P., Shafiee Ardestani, M., Mortazavi-Derazkola, S., Bitarafan-Rajabi, A., Ghoreishi, S.M., 2019. PEG-Citrate dendrimer second generation: is this a good carrier for imaging agents in vitro and in vivo? IET Nanobiotechnol. 13, 560–564.

Monedeiro, F., Pomastowski, P., Milanowski, M., Ligor, T., Buszewski, B., 2019. Monitoring of bactericidal effects of silver nanoparticles based on protein signatures and VOC emissions from Escherichia coli and selected salivary bacteria. J. Clin. Med. 8.

Mortazavi-Derazkola, S., Reza Naimi-Jamal, M., Masoumeh Ghoreishi, S., 2016. Synthesis, characterization, and atenolol delivery application of functionalized mesoporous hydroxyapatite nanoparticles prepared by microwave-assisted co-precipitation method. Curr. Drug Deliv. 13, 1123–1129.

Moteriya, P., Chanda, S., 2020. Green synthesis of silver nanoparticles from Caesalpinia pulcherrima leaf extract and evaluation of their antimicrobial, cytotoxic and genotoxic potential (3-in-1 System). J. Inorg. Organomet. Polym Mater. 30, 3920–3932.

Naghdipari, K., Shojaei, L., Heidari, A., Heidarifard, M., Sharbati, M., Mahari, A., Hosseinzadeh-Khanmiri, R., 2019. Isochromenone-functionalized mesoporous silica hollow sphere as an efficient material for drug delivery. Polyhedron 170, 659–665.

Oryan, A., Alemzadeh, E., Moshiri, A., 2017. Burn wound healing: present concepts, treatment strategies and future directions. J. Wound Care 26, 5–19.

Oryan, A., Alemzadeh, E., Tashkhourian, J., Nami Ana, S.F., 2018. Topical delivery of chitosan-capped silver nanoparticles speeds up healing in burn wounds: a preclinical study. Carbohydr. Polym. 200, 82–92.

Oryan, A., Alemzadeh, E., Mohammadi, A.A., 2019. Application of honey as a protective material in maintaining the viability of adipose stem cells in burn wound healing: a histological, molecular and biochemical study. Tissue Cell 61, 89–97.

Paulkumar, K., Gnanajobitha, G., Vanaja, M., Rajeshkumar, S., Malarkodi, C., Pandian, K., Annadurai, G., 2014. *Piper nigrum* leaf and stem assisted green synthesis of silver nanoparticles and evaluation of its antibacterial activity against agricultural plant pathogens. Sci. World J. 2014, 829894.

Perveen, S., Nadeem, R., Rehman, S.U., Afzal, N., Anjum, S., Noreen, S., Saeed, R., Amami, M., Al-Mijalli, S.H., Iqbal, M., 2022. Green synthesis of iron (Fe) nanoparticles using Plumeria obtusa extract as a reducing and stabilizing agent: antimicrobial, antioxidant and biocompatibility studies. Arab. J. Chem. 15, 103764.

Pirtarighat, S., Ghannadnia, M., Baghshahi, S., 2019. Green synthesis of silver nanoparticles using the plant extract of Salvia spinosa grown in vitro and their antibacterial activity assessment. J. Nanostruct. Chem. 9, 1–9.

Qianqian, O., Songzhi, K., Yongmei, H., Xianghong, J., Sidong, L., Puwang, L., Hui, L., 2021. Preparation of nano-hydroxyapatite/chitosan/tilapia skin peptides hydrogels and its burn wound treatment. Int. J. Biol. Macromol. 181, 369–377.

Rafique, M., Sadaf, I., Rafique, M.S., Tahir, M.B., 2017. A review on green synthesis of silver nanoparticles and their applications. Artif. Cells Nanomed. Biotechnol. 45, 1272–1291.

Ragupathi, C., Azhagu Raj, R., Ramalingam, G., Arun Kumar, K., Mohamed Basith, N., 2016. Preparation and physicochemical characterization of Ag nanorods phytosynthesis by the Petroselinum crispum plant extract. Adv. Sci. Eng. Med. 8, 862–867.

Ramadhan, M.A.K., Balasm, A.N., Kadhem, S.B., Al-Saedi, H.F., 2021. Effect of silver nanoparticles on healing of third-degree burns infected with in laboratory mice. Macedonian Veterinary Rev. 44, 17–28.

Rautela, A., Rani, J., Debnath, M., 2019. Green synthesis of silver nanoparticles from Tectona grandis seeds extract: characterization and mechanism of antimicrobial action on different microorganisms. J. Anal. Sci. Technol. 10, 5.

Ravichandran, V., Vasanthi, S., Shalini, S., Shah, S.A.A., Tripathy, M., Paliwal, N., 2019. Green synthesis, characterization, antibacterial, antioxidant and photocatalytic activity of Parkia speciosa leaves extract mediated silver nanoparticles. Results Phys. 15, 102565.

Richard, A.S., Verma, R.S., 2021. Bioactive nano yarns as surgical sutures for wound healing. Mater. Sci. Eng. C 128, 112334.

Rizwana, H., Bokahri, N.A., Alkhattaf, S., Albasher, G., Aldehaish, A.H., 2021. Antibacterial, and cytotoxic activities of silver nanoparticles synthesized from aqueous extracts of mace-arils of Myristica fragrans. Molecules 26.

Sabouri, Z., Akbari, A., Hosseini, H.A., Khatami, M., Darroudi, M., 2021. Green-based bio-synthesis of nickel oxide nanoparticles in Arabic gum and examination of their cytotoxicity, photocatalytic and antibacterial effects. Green Chem. Lett. Rev. 14, 404–414.

Salem, S.S., Fouda, A., 2021. Green synthesis of metallic nanoparticles and their prospective biotechnological applications: an overview. Biol. Trace Elem. Res. 199, 344–370.

Sharifi-Rad, M., Pohl, P., Epifano, F., Álvarez-Suarez, J.M., 2020. Green synthesis of silver nanoparticles using Astragalus tribuloides Delile. Root Extract: characterization, antioxidant, antibacterial, and anti-inflammatory activities. Nanomaterials (Basel) 10.

Sharma, K., Guleria, S., Razdan, V.K., 2020. Green synthesis of silver nanoparticles using Ocimum gratissimum leaf extract: characterization, antimicrobial activity and toxicity analysis. J. Plant Biochem. Biotechnol. 29, 213–224.

Sharma, P., Pant, S., Rai, S., Yadav, R.B., Sharma, S., Dave, V., 2018. Green synthesis and characterization of silver nanoparticles by Allium cepa L. to produce silver nano-coated fabric and their antimicrobial evaluation. Appl. Organomet. Chem. 32, e4146.

Shirzadi-Ahodashti, M., Mizwari, Z.M., Hashemi, Z., Rajabalipour, S., Ghoreishi, S.M., Mortazavi-Derazkola, S., Ebrahimzadeh, M. A., 2021. Discovery of high antibacterial and catalytic activities of biosynthesized silver nanoparticles using C. fruticosus (CF-AgNPs) against multi-drug resistant clinical strains and hazardous pollutants. Environ. Technol. Innov. 23, 101607.

Sood, R., Chopra, D.S., 2018. Optimization of reaction conditions to fabricate Ocimum sanctum synthesized silver nanoparticles and its application to nano-gel systems for burn wounds. Mater. Sci. Eng. C 92, 575–589.

Suchomel, P., Kvitek, L., Prucek, R., Panacek, A., Halder, A., Vajda, S., Zboril, R., 2018. Simple size-controlled synthesis of Au nanoparticles and their size-dependent catalytic activity. Sci. Rep. 8, 4589.

Tang, E.L., Rajarajeswaran, J., Fung, S., Kanthimathi, M.S., 2015. Petroselinum crispum has antioxidant properties, protects against DNA damage and inhibits proliferation and migration of cancer cells. J. Sci. Food Agric. 95, 2763–2771.

Tian, J., Wong, K.K., Ho, C.M., Lok, C.N., Yu, W.Y., Che, C.M., Chiu, J.F., Tam, P.K., 2007. Topical delivery of silver nanoparticles promotes wound healing. ChemMedChem 2, 129–136.

Tyavambiza, C., Elbagory, A.M., Madiehe, A.M., Meyer, M., Meyer, S., 2021. The antimicrobial and anti-inflammatory effects of silver

nanoparticles synthesised from cotyledon orbiculata aqueous extract. Nanomaterials (Basel) 11.

Veisi, H., Tamoradi, T., Karmakar, B., Mohammadi, P., Hemmati, S., 2019. In situ biogenic synthesis of Pd nanoparticles over reduced graphene oxide by using a plant extract (Thymbra spicata) and its catalytic evaluation towards cyanation of aryl halides. Mater. Sci. Eng. C 104, 109919.

Wang, Y., Beekman, J., Hew, J., Jackson, S., Issler-Fisher, A.C., Parungao, R., Lajevardi, S.S., Li, Z., Maitz, P.K.M., 2018. Burn injury: challenges and advances in burn wound healing, infection, pain and scarring. Adv. Drug Deliv. Rev. 123, 3–17.

Waris, A., Din, M., Ali, A., Ali, M., Afridi, S., Baset, A., Ullah Khan, A., 2021. A comprehensive review of green synthesis of copper oxide nanoparticles and their diverse biomedical applications. Inorg. Chem. Commun. 123, 108369.

Yaqoob, A.A., Umar, K., Ibrahim, M.N.M., 2020. Silver nanoparticles: various methods of synthesis, size affecting factors and their potential applications–a review. Appl. Nanosci. 10, 1369–1378.

Zare-Bidaki, M., Aramjoo, H., Mizwari, Z.M., Mohammadparast-Tabas, P., Javanshir, R., Mortazavi-Derazkola, S., 2022. Cytotoxicity, antifungal, antioxidant, antibacterial and photodegradation potential of silver nanoparticles mediated via Medicago sativa extract. Arab. J. Chem. 15, 103842.

Zare-Bidaki, M., Mohammadparast-Tabas, P., Peyghambari, Y., Chamani, E., Siami-Aliabad, M., Mortazavi-Derazkola, S., 2022. Photochemical synthesis of metallic silver nanoparticles using Pistacia khinjuk leaves extract (PKL@AgNPs) and their applications as an alternative catalytic, antioxidant, antibacterial, and anticancer agents. Appl. Organomet. Chem. 36, e6478.

Zhang, X.F., Liu, Z.G., Shen, W., Gurunathan, S., 2016. Silver nanoparticles: synthesis, characterization, properties, applications, and therapeutic approaches. Int. J. Mol. Sci. 17.

Zhang, X., Sun, H., Tan, S., Gao, J., Fu, Y., Liu, Z., 2019. Hydrothermal synthesis of Ag nanoparticles on the nanocellulose and their antibacterial study. Inorg. Chem. Commun. 100, 44–50.

Zheng, G., Zheng, M., Yang, B., Fu, H., Li, Y., 2019. Improving breast cancer therapy using doxorubicin loaded solid lipid nanoparticles: synthesis of a novel arginine-glycine-aspartic tripeptide conjugated, pH sensitive lipid and evaluation of the nanomedicine in vitro and in vivo. Biomed. Pharmacother. 116, 109006.